

# Synthesis of Equimolar Pd–Ru Alloy Nanoparticles Incorporated Mesoporous Alumina Films: A High Performance Reusable Film Catalyst

Anuradha Mitra, Debrina Jana, and Goutam De\*

Nano-Structured Materials Division, CSIR-Central Glass & Ceramic Research Institute, 196, Raja S. C. Mullick Road, Kolkata 700 032, India

## S Supporting Information

**ABSTRACT:** We report the synthesis of equimolar Pd–Ru alloy nanoparticles (NPs) incorporated mesoporous alumina films (Pd–Ru/MAF) by the sol–gel route. The synthetic strategy involves homogeneous mixing of the Pd<sup>2+</sup> and Ru<sup>3+</sup> ions in the alumina sol containing P123 micelles. Dip-coated films, prepared on ordinary glass substrates, were thermally reduced at a relatively lower temperature (500 °C) to generate equimolar Pd–Ru/MAF with a nominal molar composition of Pd:Ru:AlO<sub>1.5</sub> = 2:2:96. Electron microscopy studies revealed uniformly distributed Pd–Ru alloy NPs in a mesoporous alumina–alumina sphere composite film matrix. The P123/alumina nanocomposite acted as an excellent breeding medium to form Pd–Ru (~1:1) alloy NPs despite the poor miscibility of the two metals. Pd–Ru/MAF showed excellent catalytic performances with highest normalized rate constant values ( $5.43 \times 10^{14} \text{ min}^{-1} \text{ mol}^{-2}$ ) and possessed good reusability compared to the corresponding monometallic analogues in the reduction of aqueous 4-nitrophenol in the presence of NaBH<sub>4</sub> at 25 °C.

## 1. INTRODUCTION

The synthesis and applications of bimetallic nanoalloys have been always a fascinating area of exploitation to researchers. The high activity of bimetallic nanocatalysts in various reactions is generally attributed to the electronic interactions between metals resulting in rehybridization of the atomic orbitals of the bimetallic ensembles. It has been reported that factors such as similarities in atomic size, lattice parameters, and good miscibility<sup>1,2</sup> govern the ease of alloy formation process between two metals. Among the various transition metals, Pd and Ru NPs are being widely used as active catalysts in several organic<sup>3–5</sup> and inorganic reactions,<sup>6,7</sup> as well as efficient H<sub>2</sub> storage materials.<sup>8–10</sup> The alloy formation between these two metals forms another area of interest to researchers since the blending of two different metal atoms would result in a drastic change in their properties. However, the general techniques applied for the generation of bimetallic alloy NPs does not work well in the case of the Pd/Ru system. Recently, Awasthi et al. reported the synthesis of graphene supported Pd–Ru NPs with Ru incorporation of up to 10 mol % into a Pd crystal structure.<sup>11</sup> Sun et al.<sup>12</sup> reported a wet-chemical synthesis of Pd–Ru alloy NPs supported on C by using NaBH<sub>4</sub> as a reducing agent. Though the atomic ratio of Pd and Ru was reported to be 1.33:1, the X-ray diffraction pattern (XRD) of the Pd–Ru alloy NPs did not show any prominent shift of the peak positions. Thus, the evidence for formation of solid solutions between Pd and Ru is not very clear in their report. The bulk state phase diagram of the Pd–Ru system indicates that these two metals show very poor miscibilities over a wide compositional range.<sup>13</sup> Yu et al. reported a rigorous micelle-hosted synthesis for the generation of Pd<sub>0.5</sub>Ru<sub>0.5</sub> NPs<sup>14</sup> in the powder form with prominent shifting in the XRD pattern confirming the formation of a solid solution.

Another area of concern using these precious metals is their separation and reusability after a catalytic reaction. The use of bare or supported NPs in powder forms involves several problems such as uncontrolled growth of NPs, aggregate formation during catalysis, and separation after the reaction, etc. Incorporation of metal NPs in suitable matrices in film forms has been already established by our group<sup>7,15–19</sup> to be an efficient method of dealing with such problems. In a few recent reports we showed catalytic activities of mesoporous alumina (both ordered and wormhole type pores) films incorporated with different metal NPs.<sup>7,15–19</sup> The mesoporous materials not only offer high surface area allowing enhanced diffusion of reactant molecules but also provide a confined micro/nanoenvironment to the growth of metal NPs inside them.<sup>15,20,21</sup>

The vast importance of the material and the scanty reports on the synthesis of equimolar Pd–Ru nanoalloy encouraged us to explore this area. In fact, to the best of our knowledge, mesoporous alumina supported equimolar Pd–Ru nanoalloy films have not yet been synthesized. Herein, we report a simple synthetic strategy for the generation of Pd–Ru alloy nanoparticle-incorporated mesoporous alumina films via a micelle-assisted sol–gel method followed by thermal reduction. The films were characterized by GIXRD and electron microscopy. The Pd–Ru alloy NP-doped films have been exploited as a potential reusable catalyst in the reduction of 4-nitrophenol in comparison to the monometallic analogues. In fact, the Pd–Ru alloy NP-doped films show the highest normalized rate constant value for the above reaction reported so far.

**Received:** June 11, 2013

**Revised:** October 7, 2013

**Accepted:** October 14, 2013

**Published:** October 14, 2013

## 2. EXPERIMENTAL SECTION

**2.1. Materials.** Aluminum tri-*sec*-butoxide  $\text{Al}[\text{OCH}(\text{CH}_3)\text{-C}_2\text{H}_5]_3$  (ASB), ethanol, and 4-nitrophenol ( $4\text{-C}_6\text{H}_4\text{NO}_2$ ) were supplied by Merck. Pluronic P123 ( $\text{EO}_{20}\text{PO}_{70}\text{EO}_{20}$ , EO = ethylene oxide, PO = propylene oxide) and sodium borohydride ( $\text{NaBH}_4$ ) were purchased from Sigma-Aldrich while palladium chloride ( $\text{PdCl}_2$ ), acetyl acetone (acac), 1-propanol, 2-butanol, and  $\text{HNO}_3$  were obtained from s.d. Fine-Chem Ltd. Ruthenium chloride ( $\text{RuCl}_3 \cdot 3\text{H}_2\text{O}$ ) was purchased from Sisco Research Lab, and HCl was procured from Rankem. Milli-Q (Millipore) water (18.2 M $\Omega$ ) was used throughout the study. All the chemicals were used without any further purification. 1-Propanol and 2-butanol contain 0.1–0.2 wt % of water as certified by the company.

**2.2. Preparation of ASB Stock Solution.** A partially acetylacetonato-chelated ASB alumina precursor solution was prepared following the procedure reported in our previous papers.<sup>15,16</sup> Required amounts of ASB were transferred rapidly to a mixture of acetyl acetone, 1-propanol, and 2-butanol under stirring condition at room temperature such that the concentration of ASB in the ASB stock solution was ~35 wt % and the molar ratio of acac:ASB was 1:0.5. The stirring was continued for another 1 h under closed condition. This modified ASB solution was aged in closed condition at room temperature ( $25 \pm 1$  °C) for about 6 days, and used as the alumina precursor.

**2.3. Preparation of Mesoporous Alumina Sols and Films.** In a typical synthesis, 0.4 g of Pluronic P123 was dissolved in 2.0 g of ethanol and stirred for 2 h at room temperature. Then 0.7 g of 70 wt %  $\text{HNO}_3$  and 2.915 g of alumina precursor was added into the above solution. The molar ratio of  $\text{ASB}_{0.5\text{acac}}/\text{P123}/\text{EtOH}/\text{HNO}_3$  was 1:0.015:10.4:1.72. The resultant mixture was stirred for 2 h and the homogeneous mesoporous alumina sol was named MAS.<sup>22</sup> This sol was used for preparation of metal-doped mesoporous alumina films. The coatings using MAS were prepared on ordinary soda-lime glass substrates and on single-side polished Si wafers using the dipping technique (Dip-Master 200, Chemat Corporation, USA) with a withdrawal velocity of 8 in.  $\text{min}^{-1}$ . The films were dried for 16 h at 60 °C, followed by heating at 500 °C in air (ramp: 1 °C  $\text{min}^{-1}$ ) with a holding time of 2 h to eliminate all the organics. The mesoporous alumina film will be henceforth designated as MAF.

**2.4. Preparation of Pd–Ru-Doped Mesoporous Alumina Films.** For the preparation of bimetallic Pd–Ru incorporated films, first the required amounts of  $\text{PdCl}_2$  and  $\text{RuCl}_3$  dissolved in a minimum amount of 1 N HCl were mixed for 10 min. This solution was then mixed with the MAS and stirred for 1 h to get a homogeneous solutions. A 2 mol % sample of each Ru and Pd with respect to equivalent  $\text{AlO}_{1.5}$  was doped into MAS. The thin films were made by dip-coating the mixture on soda lime and silica glasses with a withdrawal velocity of 8 in.  $\text{min}^{-1}$ . The films were dried overnight at 60 °C and heated slowly (1.0 °C  $\text{min}^{-1}$ ) at 500 °C in air for 2 h. The air-annealed films were further heat-treated with a ramp of 1.5 °C  $\text{min}^{-1}$  at 500 °C for 2 h in 10%  $\text{H}_2$ –90% Ar atmosphere to reduce the metal ions. Similarly, films containing only 4 mol % of Pd and 4 mol % Ru with respect to equivalent  $\text{AlO}_{1.5}$  were also prepared separately under same reaction conditions for comparative studies. The Pd, Ru, and Pd–Ru NPs doped films

will be henceforth designated as Pd MAF, Ru MAF, and Pd–Ru MAF.

**2.5. Catalytic Study.** The catalytic properties of the Ru MAF, Pd MAF, and Pd–Ru MAF were studied by using the reduction of 4-nitrophenol as a model system. Two pieces of both side-coated catalytic films having dimensions of 1.4 cm (length)  $\times$  0.7 cm (breadth)  $\times$  0.3  $\mu\text{m}$  (thickness) were placed inside the cuvette cell of UV–visible spectrometer containing 4-nitrophenol (0.1 mL;  $3 \times 10^{-4}$  M), water (2.8 mL), and  $\text{NaBH}_4$  (0.1 mL; 0.3 M). The progress of the reaction was studied at 25 °C. The reaction mixture was stirred continuously, and the films were cautiously kept in such a way that they did not touch each other thereby ensuring maximum surface area for catalysis. After the reaction, the catalytic films were taken out, washed with water, dried at 60 °C for 10–15 min, and reused.

**2.6. Characterization.** Film thickness was measured by a Surfcoorder SE-2300 profilometer (Kosaka Laboratory Ltd.) as well as a J. A. Woolam Co. M2000 spectroscopic ellipsometer. BET measurement ( $\text{N}_2$  adsorption–desorption) was carried out using a Quantachrome Autosorb iQ Station 1 at  $-196$  °C. The sample was degassed under vacuum at 250 °C for 2 h prior to measurement.<sup>23</sup> The low and high angle grazing incidence X-ray diffraction (GIXRD) of the films were collected with a Rigaku Smart Lab (9 kW) X-ray diffractometer using  $\text{Cu K}\alpha$  radiation ( $\lambda = 1.54059$  Å). Transmission electron microscopic (TEM) images were taken using a Tecnai G<sup>2</sup> 30ST (FEI) operating at 300 kV transmission electron microscope. For TEM studies, both the undoped and Pd–Ru-doped film samples heat-treated at 500 °C were scratched off from the substrates and placed on the carbon-coated Cu grids and analyzed. The energy dispersive X-ray analyses (EDX) of samples were analyzed by the EDX facilities attached with TEM. EDX of a few single NPs were also done to evaluate the Pd/Ru composition of alloy. The reduction of 4-nitrophenol was studied using a Cary 50 scan UV–visible spectrometer at 25 °C attached with a Peltier temperature controller.

## 3. RESULTS AND DISCUSSION

Transparent films prepared from the Pd, Ru, and Pd–Ru-doped MAS sols were dried at 60 °C, followed by heat treatment at 500 °C in air which assured the complete removal of organic residues of the surfactant.<sup>16</sup> Further heating at 500 °C in reducing atmosphere (10%  $\text{H}_2$ –90% Ar) led to the generation of metallic Pd, Ru, and Pd–Ru NPs. Pd–Ru and Ru NP-doped films were yellowish brown, whereas Pd-doped film showed dark brown color (see Figure S1, Supporting Information). The low-angle X-ray diffraction (XRD) patterns of the Pd–Ru MAF (heated at 500 °C in reducing atmosphere) along with the corresponding undoped MAF are shown in Figure 1. In both cases the existence of a prominent peak at  $0.84^\circ$  ( $d \approx 10.4$  nm) and a shoulder at  $1.3^\circ$  ( $d = 7.1$  nm) confirms the presence of mesopores; however, the positions of these two peaks do not correspond to any ordered pore structure.<sup>15,16</sup> During the synthetic process, micellization of P123 takes place leading to the generation of micellar structures in the sol stage. This, on thermal treatment in the presence of air, formed mesopores owing to the removal of P123. To understand the mesoporosity we performed BET measurements of the undoped MAF material.<sup>23</sup> The  $\text{N}_2$  adsorption–desorption studies show typical type IV isotherm (H1 hysteresis loop)<sup>24</sup> characteristics to the typical mesoporous material having a surface area value of 279  $\text{m}^2 \text{g}^{-1}$  and an average pore size  $\approx 11.4$  nm (see Figure S2 in

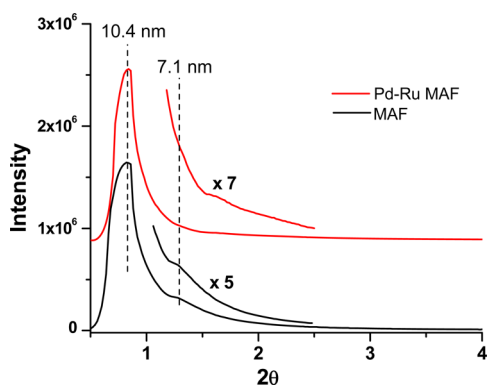


**Figure 1.** Low-angle X-ray diffraction patterns of Pd–Ru MAF and undoped MAF films heated at 500 °C confirm the presence of mesopores in the alumina matrix.

the Supporting Information). The presence of a broad low-angle XRD peak of undoped MAF having a  $d$  value of  $\sim 10.4$  nm (Figure 1) matches well with the BET result. Figure 2

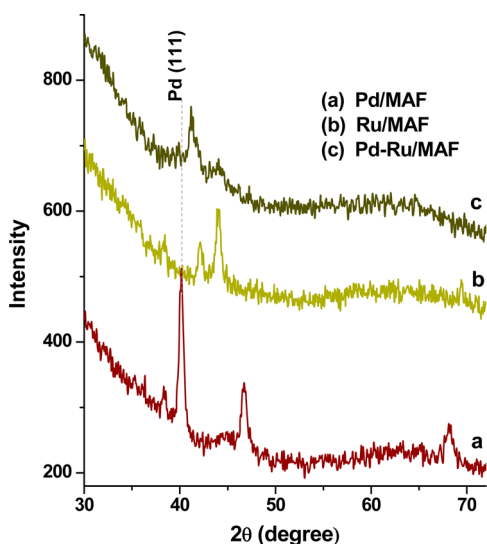


**Figure 2.** High angle X-ray diffraction patterns of Pd MAF (a), Ru MAF (b), and Pd–Ru MAF (c) heat-treated at 500 °C in 10% H<sub>2</sub>–90% Ar atmosphere. Y-axis has been shifted for clarity.

shows the high angle X-ray diffraction patterns of Pd MAF, Ru MAF, and Pd–Ru MAF films. The Pd NPs (Figure 2a) were found to possess face centered cubic (fcc) crystal structures (JCPDS no. 01-075-6724) while the alumina supported Ru NPs (Figure 2b) showed a diffraction pattern corresponding to the hexagonal closed-packed (hcp) lattice (JCPDS no. 01-089-4903). The Pd–Ru NPs copod film (Figure 2c) shows the most intense peak at 41.259° ( $d = 2.1862$  Å) which is clearly shifted to higher  $2\theta$  value with respect to the (111) peak of Pd (Figure 2a) at 40.14° ( $d_{111} = 2.2445$  Å). The position of the diffraction peak in the Pd–Ru system is exactly the same as that reported by Yu et al.<sup>14</sup> The shifting of the peak indicates the formation of a solid solution involving the incorporation of Ru atoms into the fcc structure of Pd as reported by others.<sup>4,14,25</sup> So the most intense Bragg diffraction peak at 41.259°  $2\theta$  may be considered as the reflection of the Pd–Ru (111) plane. The lattice parameter ( $a$ ) of the Pd–Ru alloy has been calculated to be 3.7883 Å by using  $d_{111} = 2.1862$  Å of Pd–Ru as below:

$$a = \sqrt{h^2 + k^2 + l^2} \times d_{hkl}$$

$$= \sqrt{3} \times d_{111}$$

The decrease of  $a$  of Pd–Ru alloy compared to pure Pd ( $d_{111} = 2.2445$  Å;  $a = 3.887$  Å) can be attributed to the incorporation of the smaller Ru atoms into the lattice of Pd during the Pd–Ru alloy formation.

Further investigation of Pd–Ru MAF was done by TEM analysis. For comparison TEM of the undoped MAF was also undertaken. The low-resolution bright-field image of the undoped MAF (Figure S3a; Supporting Information) shows wormhole-like mesopores along with existence of mesoporous spherical aggregates of size ranges from 190–320 nm with an average size of 250 nm (Figure S3a; Supporting Information). The cause of the formation of such a mesoporous alumina network with spherical aggregates could be due to the formation of two different alumina network structures during the reactions of the alumina precursor in the presence of P123 under the reaction conditions.<sup>22</sup> In the case of Pd–Ru alloy NP-incorporated films the TEM studies (Figure 3a) reveal the retention of the original mesoporous alumina–alumina sphere composite structure of alumina films and the presence of homogeneously distributed metallic NPs in the range of 13 to

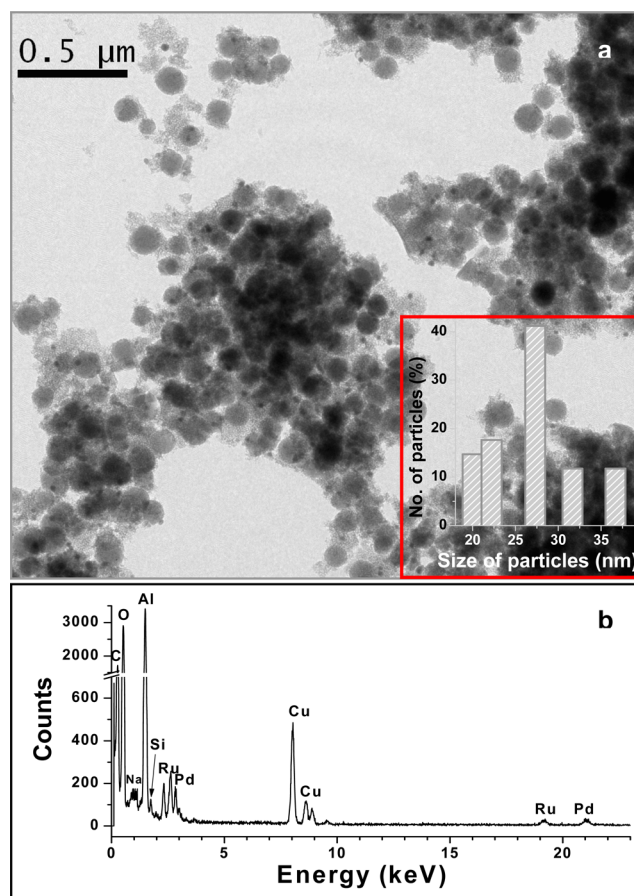


**Figure 3.** (a) TEM image of the Pd–Ru MAF sample showing alumina nanospheres cemented in the mesoporous alumina and embedded Pd–Ru alloy NPs ( $\sim \text{Pd}_{0.56}\text{Ru}_{0.44}$ ). The particle size distribution of the Pd–Ru NPs obtained from image a is shown in the inset. (b) The overall EDX spectrum recorded from the area shown in panel a. The scratched off film sample has been used for TEM studies.

37 nm with an average size of 27 nm (evaluated from the histogram shown in the inset of Figure 3a). This type of features was present in all parts of the TEM grid. Figure 3b represents the overall EDX recorded from the bright-field image in Figure 3a showing signals corresponding to Pd, Ru, Al, and O from the sample while Cu and C come from the C-coated Cu grid used for TEM study. A small amount of Si and Na are also present which must have come from the glass substrate. To understand the structure of the film more clearly, a magnified TEM image and HAADF and HRTEM images are presented in Figure 4. It is clearly seen (Figure 4a) that the

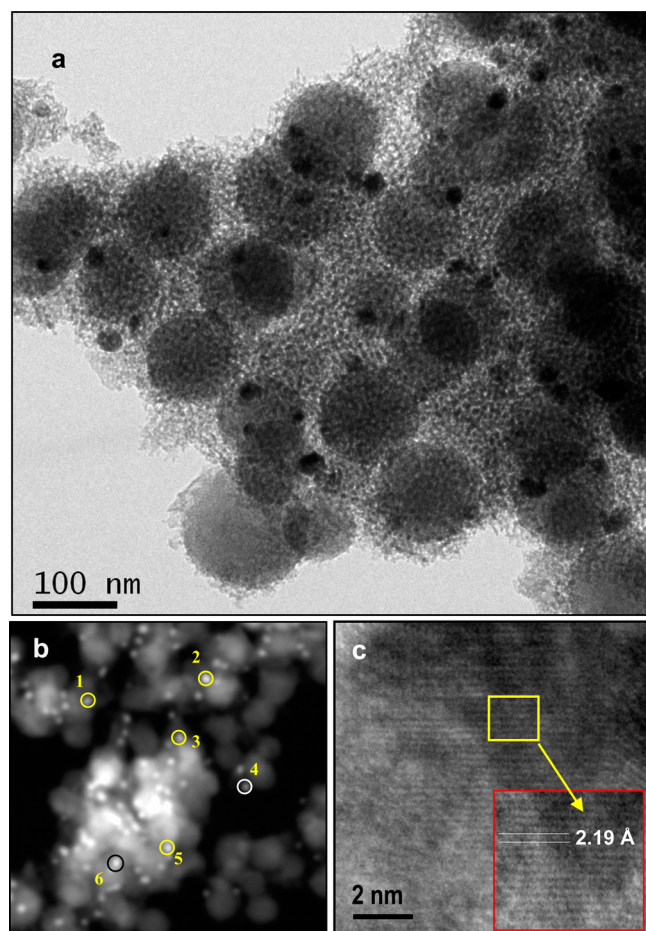


**Figure 4.** (a) Bright-field TEM image at higher magnification shows spherical metal NPs embedded in mesoporous alumina film matrix. (b) The HAADF image taken in STEM mode shows the Pd–Ru alloy NPs (brighter dots). From the encircled metal NPs quantitative point EDX were recorded. (c) The HRTEM shows crystalline nature of the NPs with fringes corresponding to the Pd–Ru alloy. The scratched off film sample has been used for TEM studies.

matrix is mesoporous and the embedded Pd–Ru metal NPs are more or less spherical in nature. Figure 4b shows the HAADF image recorded in the STEM mode showing six randomly chosen NPs on a Pd–Ru MAF sample. The single-point quantitative EDX taken from these NPs is given in Table 1. The average atomic ratio of Pd:Ru was found to be 56:44. Thus it is suggested that the bimetallic alloying between Pd and Ru has taken place with an average composition of Pd<sub>0.56</sub>Ru<sub>0.44</sub>. The HRTEM (Figure 4c) of a single particle shows lattice fringes having *d* spacing of 2.1903 Å, which is consistent with the *d*<sub>111</sub>

**Table 1. Single-Point Quantitative EDX Taken from Six Individual NPs on the HAADF Image of the Pd–Ru MAF Film (Figure 4b). The Study Shows an Average at % of Pd and Ru of 56:44 in the Alloy**

point no.	Pd (atom %)	Ru (atom %)	average Pd:Ru
1	56.85	43.14	
2	54.28	45.71	
3	55.86	44.14	56:44
4	54.91	45.09	
5	57.76	42.23	
6	57.67	42.32	

value obtained from the XRD pattern of Pd–Ru MAF (Figure 2c).

The structure of alumina network and interaction of Pd and Ru metal ions have been represented in the schematic Figure 5. Upon addition of P123 in ethanol medium, the PPO units form the inner core while PEO units constitute the outer shell of the micelle (see step a in Figure 5). In step b, the hydrolyzed polymeric alumina gets attached to the outer part of the micelle.<sup>16</sup> From the TEM we observed presence of spherical aggregates of alumina. So it is likely that two different polymeric alumina structures have been formed, the larger one (see encircled alumina network in Figure 5) formed the spherical aggregates.<sup>22</sup> The Pd<sup>2+</sup> and Ru<sup>3+</sup> ions would remain associated with the more hydrophilic PEO units of the micelle.<sup>26</sup> The dip-coated dried film (Figure 5; step c) having P123 micelles directed alumina units and loaded with Pd and Ru ions yielded equimolar Pd–Ru alloy NPs incorporated mesoporous alumina films after heat-treatment. It is noteworthy that the binary phase diagram of bulk phase Pd–Ru system suggests a maximum solubility of ~21 atom % Ru in Pd can be attained at peritectic temperature (1594 °C).<sup>13</sup> However, Yu et al. reported a rigorous micelle-hosted alloy synthesis and suggested that the micelles act as “nanoreactor” leading to the formation of Pd<sub>0.5</sub>Ru<sub>0.5</sub> NPs.<sup>14</sup> Thus, in our case it is suggested that both the Pd and Ru ions, being mixed in equimolar proportion, are entrapped inside the micelles of the MAS sol. The resultant dip-coated films are dried and heated in air followed by a subsequent thermal treatment in 10% H<sub>2</sub>–90% Ar atmosphere which leads to the 1:1 Pd–Ru alloy NPs formation embedded in mesoporous alumina film owing to their homogeneous mixing in the micellar “nanoreactor”.

The Pd–Ru MAF film was employed as catalyst in the reduction of 4-nitrophenol to 4-aminophenol by sodium borohydride. This reaction follows pseudo-first-order kinetics with respect to the concentration of the 4-nitrophenol (the concentration of borohydride being practically constant). The reaction is monitored by UV–visible spectrophotometer from the decrease in the 400 nm peak and a concomitant increase in the 300 nm peak owing to the generation of 4-aminophenol (shown in Figure 6a). The apparent rate constant (*k*<sub>app</sub>) of the reaction carried out by Pd, Ru, and Pd–Ru NP-doped films (Pd MAF, Ru MAF, and Pd–Ru MAF) were evaluated to be 0.009941, 0.017303, and 1.0909 min<sup>−1</sup>, respectively (see Figure 6b). The corresponding normalized rate constants (*k*<sub>nor</sub>) have been calculated from the above *k*<sub>app</sub> values per mole of metal NPs per mole of 4-nitrophenol (shown in Table 2). In the case of the Pd MAF, Ru MAF, and Pd–Ru MAF *k*<sub>nor</sub> is 4.9 × 10<sup>12</sup>, 8.6 × 10<sup>12</sup>, and 5.43 × 10<sup>14</sup> min<sup>−1</sup> mol<sup>−2</sup>, respectively. For comparison, we have also calculated the normalized rate constant (*k*<sub>nor</sub>) to be 1.32 × 10<sup>14</sup> min<sup>−1</sup> mol<sup>−2</sup> from the highest

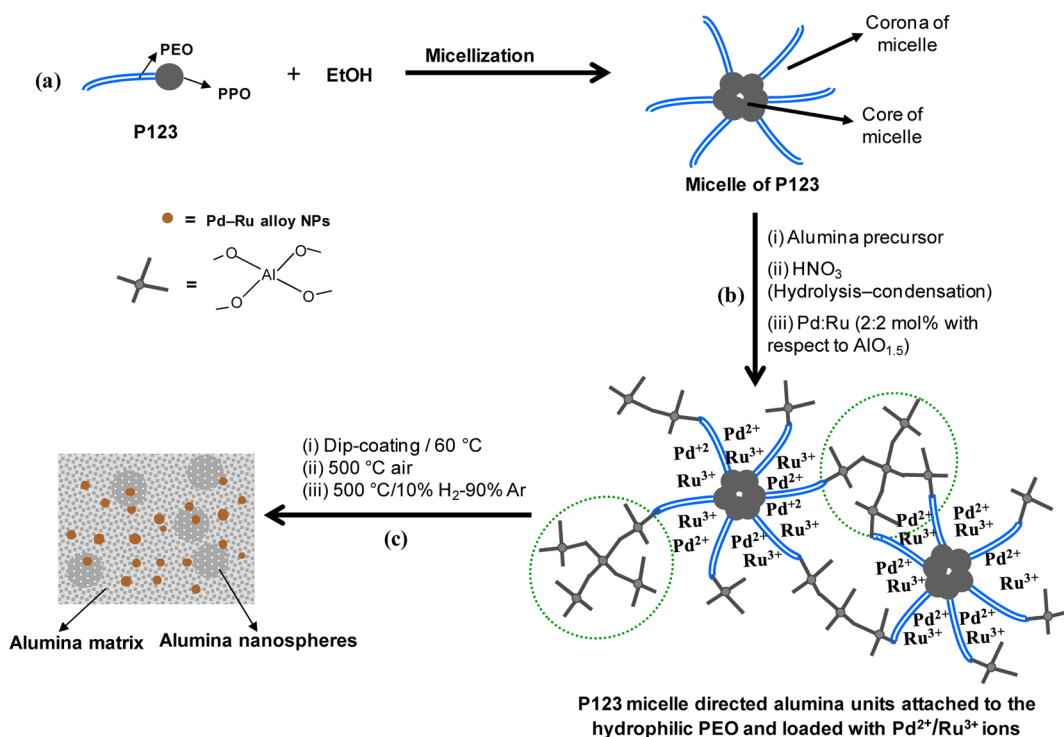


**Figure 5.** Schematic representation of alloy formation in mesoporous alumina film through (a) micellization, (b) hydrolysis–condensation of alumina precursor and entrapment of Pd<sup>2+</sup> and Ru<sup>3+</sup> ions inside P123 micelles, and (c) the generation of mesoporous alumina–alumina spheres composite network followed by Pd–Ru alloy formation upon removal of surfactants (thermal oxidation) and reduction, respectively.

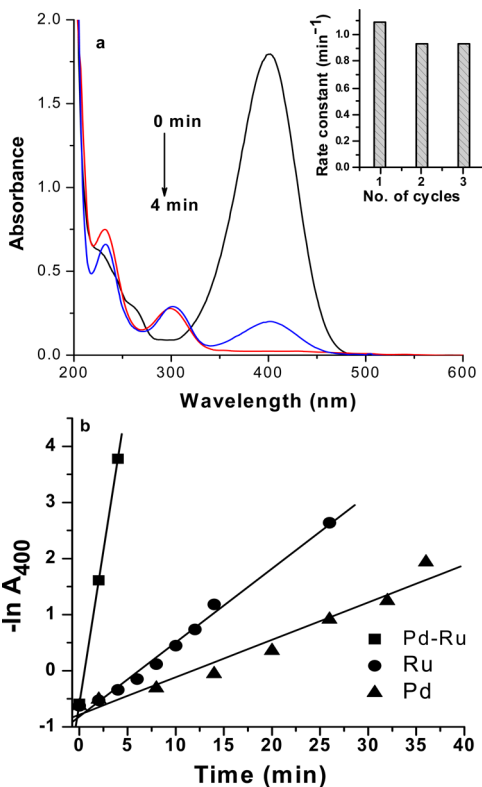


**Figure 6.** (a) Reduction of 4-nitrophenol in presence of NaBH<sub>4</sub> at 25 °C using two pieces of both-side coated Pd–Ru MAF. Dimensions of the film were 1.4 cm × 0.7 cm × 0.3 μm (thickness). The reusability of the Pd–Ru MAF catalyst is shown in the inset. (b) Comparative evaluation of rate constants for the reaction using Pd MAF, Ru MAF, and Pd–Ru MAF catalyst films.

**Table 2.** Apparent and Normalized Rate Constants of Catalysts in the Reduction of 4-Nitrophenol Reaction

entry	metal NPs	$k_{app}$ (min <sup>-1</sup> )	$k_{nor}$ (×10 <sup>14</sup> ) <sup>a</sup> (min <sup>-1</sup> mol <sup>-2</sup> )
1	Pd MAF film <sup>b</sup>	0.00994	0.049
2	Ru MAF film <sup>b</sup>	0.0173	0.086
3	Pd–Ru MAF film <sup>b</sup>	1.0909	5.43
4	Au-dendrimer nanocomposite <sup>c</sup>	0.792	1.32 <sup>c</sup>

<sup>a</sup> $k_{nor} = k_{app}/(\text{mole of metal NPs} \times \text{mole of 4-nitrophenol})$ . <sup>b</sup>Present work. <sup>c</sup>Calculated from  $k_{app}$  value of Au-dendrimer nanocomposite (sample PPI-G4; ([dendrimer]:[Au<sup>3+</sup>] = 0.7) as reported in ref 27.

$k_{app}$  value (reported so far for the conversion of 4-nitrophenol to 4-aminophenol) for the Au-dendrimer nanocomposite (sample “PPI-G4”) reported by Esumi et al.<sup>25</sup> taking into consideration the concentrations of Au NPs and the 4-nitrophenol used by them. Though the apparent rate constants (see entries 3 and 4 in Table 2) are quite close, the normalized rate constant ( $k_{nor}$ ) in the case of Pd–Ru MAF films (present work) is 5 times higher than the Au-dendrimer nanocomposite.<sup>27</sup> As a matter of fact, our catalyst film shows the highest rate constant values ( $k_{app}$  and  $k_{nor}$ ) for the aforesaid reaction reported as of now. A control study was also carried out with undoped MAF having similar coating dimensions and maintaining identical experimental conditions where no noticeable reduction was observed (see Figure S4; Supporting Information). Besides the extremely fast catalytic activity of the bimetallic Pd–Ru MAF film catalyst, it also showed an excellent reusability, presented in the inset of Figure 6a, unlike its monometallic analogues. In fact, the reusability test for the bimetallic Pd–Ru MAF was performed by simply washing these films with water followed by drying at 60 °C without any

special post-treatment method such as heating the films at 300–500 °C in inert atmosphere for regeneration of catalytic properties as reported by our group in case of Pd NPs supported on Al<sub>2</sub>O<sub>3</sub> films.<sup>7</sup> The extremely high catalytic potential and the good reusability of the bimetallic catalyst film has been discussed as follows. In the reduction of 4-nitrophenol to 4-aminophenol, two factors play key roles: (a) adsorption of hydrogen onto the surface of bimetallic NPs forming metal hydride and (b) dissociation of metal hydrides into atomic hydrogen which reduces 4-nitrophenol to 4-aminophenol.<sup>28</sup> It has been reported that Ru and Pd have a high tendency to react with H<sub>2</sub> and they are used as H<sub>2</sub> storage materials. Our group has already established that Pd NPs embedded in mesoporous film matrices such as alumina<sup>7</sup> and zirconia-modified silica<sup>29</sup> form a stable hydride (PdH<sub>x</sub>) in the presence of aqueous NaBH<sub>4</sub>. So the hydrogen (generated from the borohydride) reacts with the Pd and Ru NPs and forms relatively stable hydrides; but for enhanced catalytic reaction the instability of these metal hydrides is very important. It may be suggested that the alloy formation between Ru and Pd results in the rehybridization of the atomic orbitals of Ru and Pd atoms in such a way that the stability of the bimetallic hydride is lowered.<sup>13,30–33</sup> So, low H<sub>2</sub> dissociation energy on the surface of the Pd–Ru alloy NPs possibly accounts for the enhancement in the reaction rate as well as the reusability of catalyst film. Such high catalytic activity of a thin film of 300 nm thickness containing Pd–Ru alloy NPs is not known. Furthermore, our catalytic film can be easily separated at the end of the reaction and can be easily reused compared to the use of noble metal NPs in solution, which suffers from loss of precious metal catalysts during catalyst separation, agglomeration of the NPs, and poor reusability.

#### 4. CONCLUSIONS

In this work, we have devised a simple synthetic protocol to prepare equimolar Pd–Ru alloy NPs in alumina films at a lower temperature (500 °C). The difficulty in synthesizing such alloys in equimolar ratio owing to the immiscibility of these metals over a wide range of composition and requirement of high temperature has been successfully overcome in this work. The use of P123 directed mesoporous alumina is found to be an excellent host to obtain Pd–Ru alloy NPs in film form. The mesoporous alumina supported Pd–Ru alloy NPs film was used to investigate its catalytic behavior in the reduction of 4-nitrophenol by NaBH<sub>4</sub>. A remarkably fast reaction with the highest rate constant value along with the efficient reusability of the Pd–Ru-doped catalytic film was noted. The mechanism for the high catalytic efficiency of Pd–Ru alloy over its individual components (i.e., pure Pd and Ru films prepared under similar conditions) has been suggested. These Pd–Ru-doped films may find application as a potential reusable catalyst in electron transfer reactions.

#### ■ ASSOCIATED CONTENT

##### Supporting Information

Digital pictures of the films (Figure S1), N<sub>2</sub> adsorption–desorption isotherm and pore size distribution of the MAF material (Figure S2), TEM image of MAF heat-treated at 500 °C in air (Figure S3) and UV–visible spectra showing the inactivity of the undoped MAF toward the reduction of 4-nitrophenol in the presence of NaBH<sub>4</sub> at 25 °C (Figure S4). This material is available free of charge via the Internet at <http://pubs.acs.org>.

#### ■ AUTHOR INFORMATION

##### Corresponding Author

\*Tel: +91 33 23223403. Fax: 91 33 24730957. E-mail: [gde@cgcri.res.in](mailto:gde@cgcri.res.in).

##### Notes

The authors declare no competing financial interest.

#### ■ ACKNOWLEDGMENTS

The authors thankfully acknowledge DST, India, for financial support. We thank Dr. M. K. Naskar of Sol–Gel Division for helping in BET measurements. A.M. and D.J. thank CSIR for fellowship.

#### ■ REFERENCES

- (1) Sachtler, W. M. H.; Ertl, G.; Krozinger, H.; Weitkamp, J. *Handbook of Heterogeneous Catalysis*; VCH Wiley: Weinheim, Germany, 1997; Vol. 3.
- (2) Mavrikakis, M.; Hammer, B.; Norskov, J. K. Effect of Strain on the Reactivity of Metal Surfaces. *Phys. Rev. Lett.* **1998**, *81*, 2819.
- (3) Shao, M. H.; Huang, T.; Liu, P.; Zhang, J.; Sasaki, K.; Vukmirovic, M. B.; Adzic, R. R. Palladium monolayer and palladium alloy electrocatalysts for oxygen reduction. *Langmuir* **2006**, *22*, 10409.
- (4) Fisher, J. M.; Cabello-Moreno, N.; Christian, E.; Thompsett, D. Methanol oxidation activity of PdRu alloy nanoparticles in direct methanol fuel cells and energy conversion. *Electrochem. Solid-State Lett.* **2009**, *12*, B77.
- (5) Barrioa, V. L.; Ariasa, P. L.; Cambraa, J. F.; Güemeza, M. B.; Pawelec, B.; Fierrob, J. L. G. Hydrodesulfurization and hydrogenation of model compounds on silica–alumina supported bimetallic systems. *Fuel* **2003**, *82*, 501.
- (6) Mei, Y.; Lu, Y.; Polzer, F.; Ballauff, M. Catalytic activity of palladium nanoparticles encapsulated in spherical polyelectrolyte brushes and core–shell microgels. *Chem. Mater.* **2007**, *19*, 1062.
- (7) Dandapat, A.; Jana, D.; De, G. Pd nanoparticles supported mesoporous  $\gamma$ -Al<sub>2</sub>O<sub>3</sub> film as a reusable catalyst for reduction of toxic Cr<sup>VI</sup> to Cr<sup>III</sup> in aqueous solution. *Applied Catal. A: General* **2011**, *396*, 34.
- (8) Cheon, Y. E.; Suh, M. P. Enhanced hydrogen storage by palladium nanoparticles fabricated in a redox-active metal–organic framework. *Angew. Chem., Int. Ed.* **2009**, *48*, 2899.
- (9) Wang, L.; Yang, R. T. Hydrogen storage properties of carbons doped with ruthenium, platinum, and nickel nanoparticles. *J. Phys. Chem. C* **2008**, *112*, 12486.
- (10) Ma, L.-P.; Dai, H.-B.; Liang, Y.; Kang, X.-D.; Fang, Z.-Z.; Wang, P.-J.; Wang, P.; Cheng, H.-M. Catalytically enhanced hydrogen storage properties of Mg(NH<sub>2</sub>)<sub>2</sub> + 2LiH material by graphite-supported Ru nanoparticles. *J. Phys. Chem. C* **2008**, *112*, 18280.
- (11) Awasthi, R.; Singh, R. N. Graphene-supported Pd–Ru nanoparticles with superior methanol electrooxidation activity. *Carbon* **2013**, *51*, 282.
- (12) Sun, L.; Cao, D.; Wang, G. Pd–Ru/C as the electrocatalyst for hydrogen peroxide reduction. *J. Appl. Electrochem.* **2008**, *38*, 1415.
- (13) Kleykamp, H. Constitution and thermodynamics of the Mo–Ru, Mo–Pd, Ru–Pd and Mo–Ru–Pd systems. *J. Nucl. Mater.* **1989**, *167*, 49.
- (14) Yu, K. M. K.; Meric, P.; Tsang, S. C. Micelle-hosted bimetallic Pd–Ru nanoparticle for in situ catalytic hydrogenation in supercritical CO<sub>2</sub>. *Catal. Today* **2006**, *114*, 428.
- (15) Mitra, A.; Jana, D.; De, G. A facile synthesis of cubic (Im $\bar{3}m$ ) alumina films on glass with potential catalytic activity. *Chem. Commun.* **2012**, *48*, 3333.
- (16) Mitra, A.; Jana, D.; De, G. Facile synthesis of hexagonally ordered mesoporous aluminium oxide thin films with high catalytic activity. *Microporous Mesoporous Mater.* **2012**, *158*, 187.
- (17) Jana, D.; De, G. Spontaneous generation and shape conversion of silver nanoparticles in alumina sol, and shaped silver nanoparticle incorporated alumina films. *J. Mater. Chem.* **2011**, *21*, 6072.

(18) Jana, D.; De, G. Controlled and stepwise generation of  $\text{Cu}_2\text{O}$ ,  $\text{Cu}_2\text{O}@\text{Cu}$  and Cu nanoparticles inside the transparent alumina films and their catalytic activity. *RSC Adv.* **2012**, *2*, 9606.

(19) Jana, D.; Dandapat, A.; De, G. Au@Pd core-shell nanoparticle incorporated alumina sols and coatings: transformation of Au@Pd to Au-Pd alloy nanoparticles. *J. Phys. Chem. C* **2009**, *113*, 9101.

(20) Yuan, Q.; Duan, H.-H.; Li, L.-L.; Li, Z.-X.; Duan, W.-T.; Zhang, L.-S.; Song, W.-G.; Yan, C.-H. Homogeneously dispersed ceria nanocatalyst stabilized with ordered mesoporous alumina. *Adv. Mater.* **2010**, *22*, 1475.

(21) Lu, A.-H.; Schmidt, W.; Matoussevitch, N.; Bönnemann, H.; Spliethoff, B.; Tesche, B.; Bill, E.; Kiefer, W.; Schüth, F. Nano-engineering of a magnetically separable hydrogenation catalyst. *Angew. Chem.* **2004**, *116*, 4403.

(22) It is noteworthy to mention here that our earlier studies using P123 and freshly prepared acac modified ASB precursor yielded 2D hexagonal mesoporous alumina films using the sol composition (molar)  $\text{ASB}_{0.5\text{acac}}:\text{P123}:\text{EtOH}:\text{HNO}_3 = 1:0.015:55.13:1.72$  (equivalent  $\text{AlO}_{1.5}$  wt % in the sol was 1.35 %; see ref 16). In the present study we have used aged alumina precursor and a low amount of ethanol to make the sol more concentrated (equivalent  $\text{AlO}_{1.5}$  wt % = 3.49; see experimental section 2.3) to increase the film thickness. However, in this case the rate of hydrolysis-condensation reactions of  $\text{ASB}_{0.5\text{acac}}$  is expected to be very fast due to the high alumina content of the sol and much higher relative acid concentration, compared to our earlier work (ref 16). The formation of spherical alumina aggregates could be due to the very fast hydrolysis-condensation reactions of closely packed alumina units followed by micellization with P123 (see Figure 5). So mesoporous alumina-alumina spheres composite structure of the films could be due to such changes of experimental conditions.

(23) For BET measurements, the undoped mesoporous alumina sol (MAS) used for film deposition (MAF) was converted into gel by solvent evaporation. The gel was then dried (60 °C) and heat-treated (500 °C) following the similar way as that of film (MAF) to remove organics, and used for BET studies.

(24) Cai, W.; Yu, J.; Anand, C.; Vinu, A.; Jaroniec, M. Facile synthesis of ordered mesoporous alumina and alumina-supported metal oxides with tailored adsorption and framework properties. *Chem. Mater.* **2011**, *23*, 1147.

(25) Lu, M.; Yu, W.; Liu, H.; Zheng, J. Preparation and characterization of polymer-stabilized ruthenium-platinum and ruthenium-palladium bimetallic colloids and their catalytic properties for hydrogenation of *o*-chloronitrobenzene. *J. Colloid Interface Sci.* **1999**, *214*, 231.

(26) Khullar, P.; Singh, V.; Mahal, A.; Kaur, H.; Banipal, T. S.; Kaur, G.; Singh, V.; Bakshi, M. S. Tuning the shape and size of gold nanoparticles with triblock polymer micelle structure transitions and environments. *J. Phys. Chem. C* **2011**, *115*, 10442.

(27) Hayakawa, K.; Yoshimura, T.; Esumi, K. Preparation of gold-dendrimer nanocomposites by laser irradiation and their catalytic reduction of 4-nitrophenol. *Langmuir* **2003**, *19*, 5517.

(28) Harish, S.; Mathiyarasu, J.; Phani, K. L. N.; Yegnaraman, V. Synthesis of conducting polymer supported Pd nanoparticles in aqueous medium and catalytic activity towards 4-nitrophenol reduction. *Catal. Lett.* **2009**, *128*, 197.

(29) Saha, J.; Dandapat, A.; De, G. Transformation of Pd  $\rightarrow$   $\text{PdH}_{0.7}$  nanoparticles inside mesoporous Zr-modified  $\text{SiO}_2$  films in ambient conditions. *J. Mater. Chem.* **2011**, *21*, 11482.

(30) Rödriguez, J. A. Metal-metal bonding on surfaces: molecular orbital study of Pd/Ti(001) and Pd/Ru(001). *Surf. Sci.* **1994**, *303*, 366.

(31) Rödriguez, J. A. Electronic and chemical properties of Pt, Pd, and Ni in bimetallic surfaces. *Surf. Sci.* **1996**, *345*, 347.

(32) Greeley, J.; Mavrikakis, M. Near-surface alloys for hydrogen fuel cell applications. *Catal. Today* **2006**, *111*, 52.

(33) Hartmann, H.; Diemant, T.; Bergbreiter, A.; Bansmann, J.; Hoster, H. E.; Behm, R. Surface alloy formation, short-range order, and deuterium adsorption properties of monolayer PdRu/Ru(0001) surface alloys. *Surf. Sci.* **2009**, *603*, 1439.